^{64}Cu Treatment Planning and ^{67}Cu Therapy with Radiolabeled [^{64}Cu/^{67}Cu]MeCOSar-Octreotate in Subjects with Unresectable Multifocal Meningioma: Initial Results for Human Imaging, Safety, Biodistribution, and Radiation Dosimetry

Dale L. Bailey[1–3], Kathy P. Willowson[1,4], Matthew Harris[5], Colin Biggin[5], Alireza Aslani[1,2], Nigel A. Lengkeek[6], Jon Stoner[7], M. Enid Eslick[1], Harry Marquis[3,4], Michelle Parker[5], Paul J. Roach[1,2], and Geoffrey P. Schembri[1,2]

[1]Department of Nuclear Medicine, Royal North Shore Hospital, Sydney, New South Wales, Australia; [2]Faculty of Medicine and Health, University of Sydney, Sydney, New South Wales, Australia; [3]Sydney Vital Translational Cancer Research Centre, Sydney, New South Wales, Australia; [4]Institute of Medical Physics, University of Sydney, Sydney, New South Wales, Australia; [5]Clarity Pharmaceuticals, Sydney, New South Wales, Australia; [6]ANSTO Biosciences, Sydney, New South Wales, Australia; and [7]Idaho Accelerator Center, Idaho State University, Pocatello, Idaho

Our aim was to report the use of ^{64}Cu and ^{67}Cu as a theranostic pair of radionuclides in human subjects. An additional aim was to measure whole-organ dosimetry of ^{64}Cu and ^{67}Cu attached to the somatostatin analog octreotate using the sarcophagine MeCOSar chelator (SARTATE) in subjects with somatostatin receptor–expressing lesions confined to the cranium, thereby permitting normal-organ dosimetry for the remainder of the body. **Methods:** Pretreatment PET imaging studies were performed up to 24 h after injection of [^{64}Cu]Cu-SARTATE, and normal-organ dosimetry was estimated using OLINDA/EXM. Subsequently, the trial subjects with multifocal meningiomas were given therapeutic doses of [^{67}Cu]Cu-SARTATE and imaged over several days using SPECT/CT. **Results:** Five subjects were initially recruited and imaged using PET/CT before treatment. Three of the subjects were subsequently administered 4 cycles each of [^{67}Cu]Cu-SARTATE followed by multiple SPECT/CT imaging time points. No serious adverse events were observed, and no adverse events led to withdrawal from the study or discontinuation from treatment. The estimated mean effective dose was 3.95×10^{-2} mSv/MBq for [^{64}Cu]Cu-SARTATE and 7.62×10^{-2} mSv/MBq for [^{67}Cu]Cu-SARTATE. The highest estimated organ dose was in spleen, followed by kidneys, liver, adrenals, and small intestine. The matched pairing was shown by PET and SPECT intrasubject imaging to have nearly identical targeting to tumors for guiding therapy, demonstrating a potentially accurate and precise theranostic product. **Conclusion:** ^{64}Cu and ^{67}Cu show great promise as a theranostic pair of radionuclides. Further clinical studies will be required to examine the therapeutic dose required for [^{67}Cu]Cu-SARTATE for various indications. In addition, the ability to use predictive ^{64}Cu-based dosimetry for treatment planning with ^{67}Cu should be further explored.

Key Words: radionuclide therapy; copper radionuclides; dosimetry; meningioma; safety; theranostics

J Nucl Med 2023; 64:704–710
DOI: 10.2967/jnumed.122.264586

A proposed pair of radionuclides potentially ideal for theranostics is ^{64}Cu and ^{67}Cu (*1*). ^{64}Cu has a 12.7-h physical half-life and emits positrons (β^+) with a maximum energy of 0.65 MeV at 17% abundance, making it suitable for imaging with PET. ^{67}Cu decays by β^- emissions in the range of 0.18–0.58 MeV at 100% abundance and emits readily imageable γ-photons at 0.092 MeV (23%) and 0.185 MeV (49%) with a physical half-life of 61.8 h. As both radionuclides are elemental copper, the chemistry for chelating the imaging agent and the therapeutic compound is essentially identical. ^{64}Cu is made in a cyclotron, and yields can be realized so that patient doses can be provided on a commercial scale. ^{67}Cu is produced by high-energy x-rays from an electron accelerator via the ^{68}Zn(γ,p)^{67}Cu reaction (*2*). Moreover, the chelation chemistry of radiolabeled copper is well developed (*1*). Given these recent chelation and production developments, there is currently significant interest in the use of ^{64}Cu/^{67}Cu as a theranostic pair (recently termed targeted copper theranostic).

The ^{64}Cu/^{67}Cu pairing offers significant advantages over theranostic pairs such as ^{68}Ga/^{177}Lu, including the fact that the extended physical half-lives of both ^{64}Cu and ^{67}Cu permit centralized production and widespread transportation of ready-to-use theranostic agents for both diagnosis and therapy to remote sites, which is generally not possible with generator-produced ^{68}Ga. Another advantage is the scalable product supply for ^{64}Cu and ^{67}Cu due to favorable production methods using cyclotrons and accelerators, respectively. In addition, ^{64}Cu can be imaged on the day of administration (as with current PET radionuclides such as ^{68}Ga) but also offers the ability to collect images up to 48 h after administration for flexible patient scheduling and potentially improved lesion identification. ^{67}Cu emits abundant γ-photons, which are well suited for SPECT imaging, as well as a β^- particle for therapy with an energy and pathlength in tissue similar to those of ^{177}Lu. ^{67}Cu also has a shorter half-life (2.6 d) than ^{177}Lu (6.7 d), making it well matched to peptide pharmacokinetics presenting less of a radiation protection challenge and may allow more frequent administrations. A final advantage is that the longer physical half-life of ^{64}Cu than of

Received Jun. 28, 2022; revision accepted Nov. 28, 2022.
For correspondence or reprints, contact Dale L. Bailey (dale.bailey@sydney.edu.au).
Published online Dec. 2, 2022.

^{68}Ga improves the ability to obtain pretherapy dosimetry estimates using PET imaging at multiple time points, potentially leading to a personalized treatment approach.

In this paper, we report the first-in-humans use of ^{64}Cu and ^{67}Cu as a theranostic pair for treatment planning and therapy. The primary aims of the study were to assess the safety, biodistribution, and dosimetry of both copper radionuclides labeled to the somatostatin analog Tyr^3-octreotate (H-D-Phe-Cys-Phe-D-Trp-Lys-Thr-Cys-Thr-OH) conjugated to the MeCOSar sarcophagine chelator (SARTATE) (*3*). The design was an open-label, nonrandomized phase I safety study on adults with meningiomas using fixed dosing of both the diagnostic and the therapeutic investigational medical products, [^{64}Cu]Cu-SARTATE and [^{67}Cu]Cu-SARTATE, respectively. [^{64}Cu]Cu-SARTATE binds to tumors expressing somatostatin receptor type 2 (*4*), which has been shown to be overexpressed in meningiomas (*5*). This population was selected for the study because of the high unmet clinical need and the expected normal uptake in organs outside the calvarium, thus permitting normal-organ dosimetry measures, which is not the case with typical somatostatin receptor type 2–expressing cancers in subjects with metastatic neuroendocrine tumors.

MATERIALS AND METHODS

Production of Radionuclides of Copper

[^{64}Cu]$CuCl_2$ was manufactured on a biomedical cyclotron (PET Trace; GE Healthcare) via the ^{64}Ni(p,n)^{64}Cu nuclear reaction and subsequently was purified on an automated synthesizer (Comecer) (*6*).

[^{67}Cu]$CuCl_2$ was obtained by irradiation of enriched ^{68}Zn targets at 40 MeV on a linear electron accelerator (Idaho Accelerator Center) via the reaction process ^{68}Zn(γ,p)^{67}Cu. After irradiation, zinc and copper are separated by low-pressure evaporation and subsequently purified using anion-exchange column chromatography. The final product pH was adjusted to 2.0 (nominal), and volume activity was more than 40 MBq/μL (~1 mCi/μL). Typical specific activities were greater than 7 TBq/mg (~200 Ci/mg).

Subject Selection and Recruitment

The subjects had unresectable, multifocal meningiomas that were progressing despite chemotherapy and radiotherapy. The cranial localization of the disease enables assessment of the normal biodistribution in the visceral organs—with little prospect of the disease being present or affecting biodistribution—to derive normal-organ dosimetry. Previous studies using [^{64}Cu]Cu-SARTATE in humans (*4*) recruited neuroendocrine tumor subjects for whom metastatic disease was often present throughout the abdomen and in organs such as liver and pancreas and, thus, for whom estimation of normal-organ dosimetry was not always possible. Using subjects with cranial lesions avoids this issue. The study (ClinicalTrials.gov identifier NCT03936426) was approved by a nationally accredited Human Research Ethics Committee (St. Vincent's Hospital Melbourne HREC, reference number HREC/17/SVHM/238), and written informed consent was obtained from all subjects before recruitment.

Imaging Studies

Before the trial began, the quantitative accuracy of the PET scanner (Biograph mCT/64; Siemens Healthineers) was validated with a modified version of the protocol developed by our national imaging clinical trials group (the Australasian Radiopharmaceutical Trials Network) (*7*) adapted for ^{64}Cu PET imaging. The protocol used a National Electrical Manufacturers Association NU-2 image-quality phantom and demonstrated the SUV_{mean} in the main compartment of the phantom to be accurate to within ±5% of the true value of 1.0 (i.e., SUV = 0.95–1.05). ^{64}Cu used for the dose calibrator and camera validation was traceable to the primary Australian ^{64}Cu standard established by the national nuclear science body, the Australian Nuclear Science and Technology Organization.

[^{64}Cu]Cu-SARTATE Preparation, Administration, and Imaging. [^{64}Cu]Cu-SARTATE was prepared at a radiopharmaceutical manufacturing facility in Adelaide on day −1 and transported by plane overnight to our center in Sydney. No specific preparation was required of the subjects; in particular, no subjects were on any medication such as somatostatin analogs that could potentially interfere with uptake and biodistribution. The [^{64}Cu]Cu-SARTATE was administered on day 0 as an approximately 200-MBq slow-bolus intravenous injection. Imaging was acquired on the time-of-flight PET/CT system with a 21.6-cm axial field of view in fully 3-dimensional acquisition mode at multiple time points after administration: 1, 4, and 24 h. On day 0, scans were acquired for 3 min per bed position with coverage from the vertex of the skull to the mid thigh. To partially compensate for radionuclide decay, on day +1 the acquisition time was extended to 5 min per bed position. Image reconstruction used CT-based scatter and attenuation correction, time-of-flight localization, and a resolution recovery algorithm (TrueX; Siemens Healthineers) followed by a post-reconstruction gaussian 3-dimensional filter with a full width at half maximum of 5.0 mm.

[^{67}Cu]Cu-SARTATE Preparation, Administration, and Imaging. [^{67}Cu]Cu-SARTATE was manufactured on-site in our local hospital radiopharmacy facility using the imported ^{67}Cu. The trial protocol was designed so that a reliable, repeatable administration of a minimum of 5 GBq of [^{67}Cu]Cu-SARTATE was achievable.

Briefly, the [^{67}Cu]Cu-SARTATE was prepared manually by the reaction of [^{67}Cu]$CuCl_2$ in 0.1 M HCl with SARTATE (60 μg, good-manufacturing-practice grade; Auspep Clinical Peptides) according to previously optimized methods for production and quality control. The purity and safety of the product for release were assessed with radio–thin-layer chromatography, radio–high-performance liquid chromatography, and testing of pH, pyrogenicity, sterile filter integrity, and post-release sterility.

The subjects in this trial received the [^{67}Cu]Cu-SARTATE as a ramped, slow infusion over 20 min. All subjects had coadministration of 1 L of amino acid solution (5.8 g of lysine and 11.5 g of arginine per liter) over 3–4 h for renal protection commencing 30 min before the [^{67}Cu]Cu-SARTATE administration. Regular clinical observations, including electrocardiography, were made from the time of administration. The subjects were asked to void their bladder before the injection and not to void again until after the first scan at +1 h, to allow a cross-check of the total radioactivity in the reconstructed images and comparison with the known amount of ^{67}Cu injected. All ^{67}Cu imaging was performed as whole-body SPECT/CT scans on a dual-detector γ-camera (Intevo.6; Siemens Healthineers), with a thicker scintillation detector (16 mm) than is standard, for increased sensitivity for medium- and higher-energy photons such as from ^{67}Cu. Scanning proceeded from the vertex of the skull to the mid thigh, and quantitative SPECT images subsequently were reconstructed using in-house protocols and software (*8*). A calibration source (~125 mL) containing about 40 MBq of ^{67}Cu was included in 1 bed position at each time point. The acquisition consisted of 3 contiguous bed positions, each being approximately 38 cm in axial extent. Imaging was acquired on days 0, +1, and +4 at the approximate time points of 1, 4, 24, and 96 h after administration. In addition, on day +1, a 2-dimensional planar anterior/posterior whole-body sweep was acquired. Images were acquired using a medium-energy collimator with the main pulse-height analyzer window over the 185 keV ± 10% photopeak and a lower-energy scatter window (143–163 keV). All SPECT data were acquired using continuous detector rotation into 120 projections over 360° in a 128 × 128 matrix. The time per projection varied; for both acquisitions on day 0 (1 and 4 h

after infusion), it was 8 s/projection; on day +1, it was 10 s/projection; and on day +4, it was 12 s/projection. Images were reconstructed using the ordered-subset expectation maximization algorithm (*9*) after scatter correction in projection space using an in-house implementation of the transmission-dependent scatter correction method (*8,10*). The reconstruction took place on a dedicated nuclear medicine workstation (Hermes Medical Solutions AB) and was followed by attenuation correction based on the CT scan using a modified version of the method of Chang (*8,11*). Finally, the images were converted to units of kBq/cc for further analysis.

The complete set of data acquired for the [^{64}Cu]Cu-SARTATE PET before treatment and the [^{67}Cu]Cu-SARTATE for each cycle provided 3 PET/CT scans and 16 (4 cycles × 4 time points per cycle) whole-body SPECT/CT scans per individual for analysis.

Biodistribution and Radiation Dosimetry

Both the PET data and the SPECT data were processed to determine organ biodistribution over time and whole-body radiation dosimetry. Organs of interest were defined on the CT and functional (PET or SPECT) multimodality images at the baseline time point in each image series and transferred to the subsequent time points. [^{64}Cu]Cu-SARTATE and [^{67}Cu]Cu-SARTATE studies were considered separately. The ^{67}Cu calibration source in the field of view was checked for total radioactivity remaining to assess the accuracy of the quantitative SPECT images. Whole-body retention was estimated on the basis of the imaging, with an adjustment for the missing lower limbs. Organs of interest were defined for liver, spleen, kidneys, lungs, blood pool, L4–L5 spine (for bone marrow estimates), adrenal and parotid glands, urinary bladder, and small bowel using a dedicated nuclear medicine workstation (MIM Encore; MIM Software). Brain estimates of radioactivity were not included because of the presence of disease within the skull. The total uptake in each organ was calculated and converted to percentage injected dose. The blood pool estimate was scaled by the blood volume based on the concentration of the radionuclide measured in the images and the total blood volume in the models (standard MIRD adult male and female models) used in the OLINDA/EXM program (*12,13*). A similar approach was used for thigh-based muscle volume of interest. The estimate of percentage injected dose in bone marrow was based on the L4–L5 vertebrae containing about 7% of the average total bone marrow in an adult (*14,15*). The corresponding time–activity curve data were imported into the OLINDA/EXM whole-organ dosimetry package after decay correction with the respective half-lives for each radionuclide.

Dosimetry for [^{64}Cu]Cu-SARTATE and [^{67}Cu]Cu-SARTATE

All subjects who were selected to proceed to therapy had dosimetry estimates calculated for the PET imaging component of the trial. To allow direct comparison with the previously published dose estimates of a similar radiopharmaceutical, [^{64}Cu]DOTA-octreotate (*16*), we used a dynamic bladder model in the OLINDA analysis based on an estimated urinary excretion fraction of 10% with a presumed 2-h voiding interval and a biologic half-life of 1 h. The same assumptions and parameters used for the calculation of the absorbed radiation dose estimates for [^{64}Cu]Cu-SARTATE above were applied for the absorbed dose estimates from [^{67}Cu]Cu-SARTATE. All ^{67}Cu data were decay-corrected before entry into OLINDA.

RESULTS

Subject Selection and Recruitment

Five subjects (4 male, 1 female) were initially recruited to the trial, 3 of whom went on to receive the therapy. One subject did not proceed to therapy because the subject disclosed a previous malignancy (a skin lesion) after recruitment and hence did not meet the inclusion criteria. The other subject was diverted to [^{177}Lu]Lu-DOTA-octreotate treatment because of rapid disease progression and conflicts with the scheduling of the ^{67}Cu radionuclide. These 2 subjects were not included in the dosimetry calculations. All 3 remaining subjects (2 male, 1 female) had unresectable, multifocal meningiomas previously treated with radiotherapy and chemotherapy and no other malignancies. Table 1 shows the imaging data for the 3 therapy subjects at all imaging time points.

Imaging Studies

[^{64}Cu]Cu-SARTATE Preparation, Administration, and Imaging. The average amount of [^{64}Cu]Cu-SARTATE administered was 186 MBq (range, 176–207 MBq). No adverse events were recorded after the [^{64}Cu]Cu-SARTATE injection in any subject. An example set of images for 1 subject is shown in Figure 1.

[^{67}Cu]Cu-SARTATE Preparation, Administration, and Imaging. The amount of [^{67}Cu]Cu-SARTATE produced over the 12 cycles was 9,660 ± 828 MBq, and all batches were within specifications. The purity and safety of the product were measured by radio–thin-layer chromatography (average, 98.9% ± 0.6%), radio–high-performance liquid chromatography (average, 96.4% ± 2.8%), and testing of pH (7.0) and pyrogenicity (<5.0 EU/mL). Sterile filter integrity and post-release sterility were confirmed.

The 3 subjects received an average of 4,945 ± 100 MBq (range, 4,695–5,076 MBq) of [^{67}Cu]Cu-SARTATE over a combined total of 12 cycles of treatment. SPECT maximum-intensity projection images for the same subject as for Figure 1 are shown in Figure 2, with the additional time point (96 h) facilitated by the longer

TABLE 1
Imaging Data Acquired at Various Time Points in All Subjects

Postadministration time (h)	^{64}Cu PET	^{67}Cu SPECT			
		Cycle 1	Cycle 2	Cycle 3	Cycle 4
~1	Yes	Yes	Yes	Yes	Yes
~4	Yes	Yes	No (2/3)	Yes	Yes
~24	Yes	Yes	Yes	Yes	Yes
~96	NA	Yes	Yes	Yes	Yes

NA = not applicable; No = not all 3 subjects were imaged at this time point; Yes = all 3 subjects were imaged at this time point.
Only 1 time point in 1 subject was omitted (subject B, cycle 2, day 0, +4 h) because of very delayed start of infusion, precluding measurement late in evening.

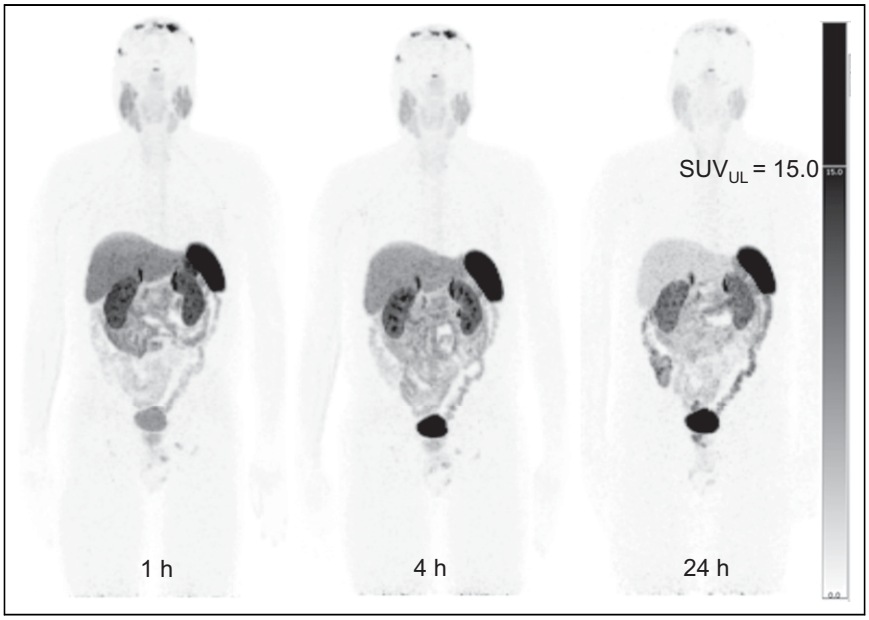

FIGURE 1. Example of multiple-time-point maximum-intensity projections with [^{64}Cu]Cu-SARTATE PET at 1, 4, and 24 h after injection. Considerable washout of radiopharmaceutical is seen from liver, parotid glands, and intracranial lesions at 24 h. Gray scale is constant for all images, with SUV display range of 0–15. SUV$_{UL}$ = upper limit of SUV.

half-life of ^{67}Cu. Figure 3 compares the uptake for both [^{64}Cu]Cu-SARTATE and [^{67}Cu]Cu-SARTATE through the largest tumor in the subject.

Safety, Biodistribution, and Radiation Dosimetry

Adverse Events. Both [^{64}Cu]Cu-SARTATE and [^{67}Cu]Cu-SARTATE were safe and well tolerated in all subjects. No serious adverse events, no potentially life-threatening (grade 4) treatment-emergent adverse events, and no deaths were recorded during the study period. Further, there were no treatment discontinuations or interruptions and no withdrawals from the study due to treatment-emergent adverse events. [^{64}Cu]Cu-SARTATE had no treatment-emergent adverse events, and [^{67}Cu]Cu-SARTATE had 16, which included 13 incidents of decreased lymphocyte count in the 3 therapy subjects. Further details of the adverse events are included in Supplemental Tables 1 and 2 (supplemental materials are available at http://jnm.snmjournals.org). There were no notable safety findings arising from review of the electrocardiographs, vital signs, or physical examination data.

Biodistribution Data. The decay-corrected radionuclide retention curves from the PET and SPECT imaging at all 4 cycles for each subject are shown in Figure 4. Whole-body retention was highly reproducible over all cycles of treatment. For the [^{67}Cu]Cu-SARTATE biodistribution, the organ that exhibited the highest total uptake expressed as percentage injected dose was liver, followed by kidney, spleen, and lungs. The averaged biodistribution for all subjects and all cycles of treatment is shown in Table 2 as the amount of the radiopharmaceutical in the organs at each time point. The individual-subject biodistribution data for each cycle and each time point are included in Supplemental Tables 3–5.

Dosimetry for [^{64}Cu]Cu-SARTATE and [^{67}Cu]Cu-SARTATE. The averaged radiation dosimetry estimates of [^{64}Cu]Cu-SARTATE for the PET and SPECT imaging components of the trial from the 3 subjects who proceeded to therapy are shown in Table 3. The highest organ dose per megabecquerel was in spleen, followed by kidneys, liver, adrenals, and small intestine. This was consistent for both [^{64}Cu]Cu-SARTATE and [^{67}Cu]Cu-SARTATE. The difference in dosimetry between the 2 SARTATE radiopharmaceuticals averaged a factor of 2.6 (range, 1.3–4.0), with the ^{67}Cu product conferring the higher dose. However, this factor was not consistent among different organs, possibly because of altered biodistribution kinetics due to the use of the amino acid infusion when administering the therapeutic product, especially in the first 4 h.

DISCUSSION

The potential clinical use of the radionuclides of copper, predominantly ^{64}Cu and ^{67}Cu, was suggested over 40 y ago (*17*). Subsequently, in 1995, Schwarz et al. reported a preclinical study on rodents bearing lymphomas examining the radiation dosimetry from ^{64}Cu and ^{67}Cu radiolabeled [Cu]benzyl-TETA-1A3 monoclonal antibody and reported a 5-fold increase in absorbed radiation dose per unit of radioactivity for the longer-lived ^{67}Cu compared with ^{64}Cu (*18*). Subsequently, DeNardo et al. reported the use of a ^{67}Cu-radiolabeled monoclonal antibody ([^{67}Cu]2IT-BAT-Lym-1)

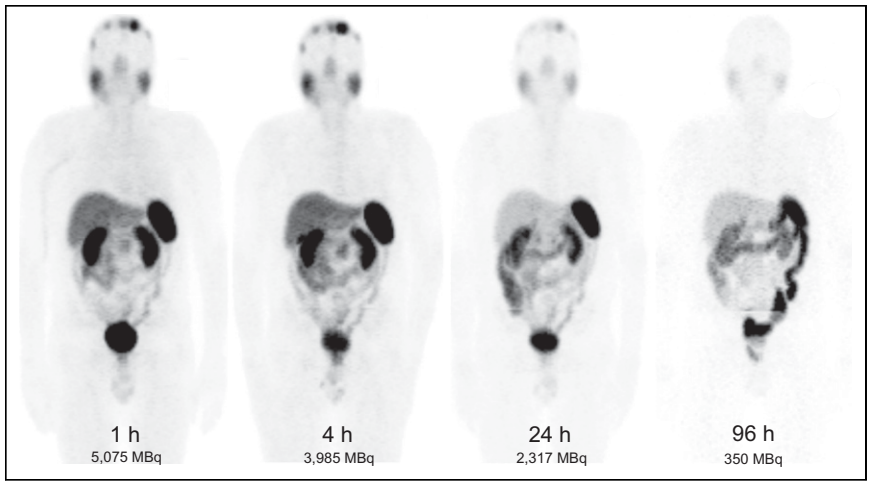

FIGURE 2. SPECT maximum-intensity projections for same subject as in Figure 1 are shown for each imaging time point in cycle 1 of treatment. Total radioactivity estimated in subject is shown at each time point. Gray scale is not constant in this example because of wide dynamic range and hence is not displayed. Good image quality with SPECT was obtained up to 96 h. Calibration standard was removed from images before display.

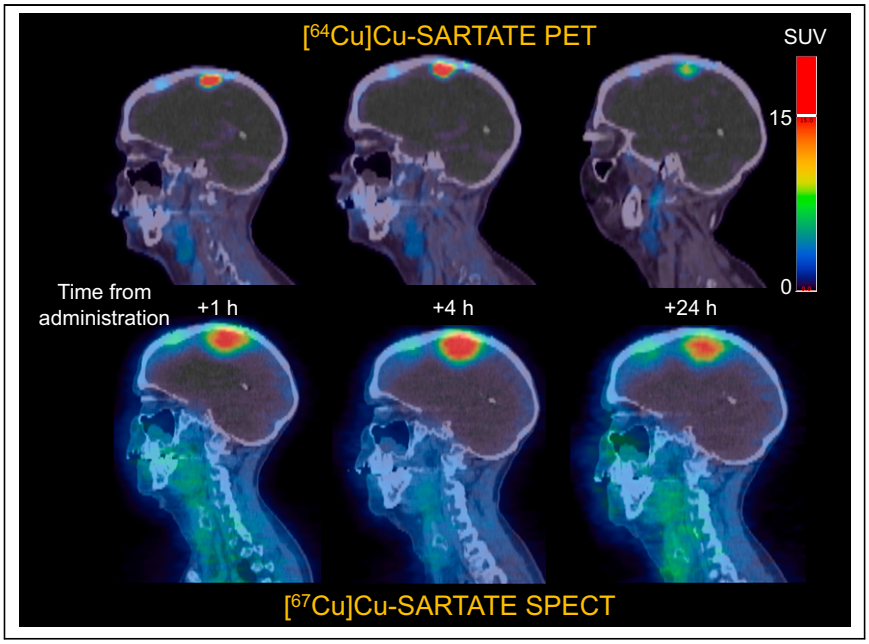

FIGURE 3. Reproducibility of copper theranostic PET and SPECT pairing is shown in this comparison of SARTATE showing targeting of 2 compounds using PET and SPECT at equivalent time points after administration. Change of radionuclide from ^{64}Cu to ^{67}Cu does not alter targeting to tumor in this subject. SPECT images are from cycle 1 of treatment. Volume of main lesion in SPECT images appears greater than in PET images because of poorer spatial resolution of SPECT. PET images are shown at fixed SUV upper threshold (maximum, 15), whereas SPECT images are shown with individual scaling. SPECT time point of 96 h has been omitted as there was no comparable PET image.

in subjects with stage 3 or 4 B-cell lymphoma to assess feasibility for subsequent treatment (*19,20*). Remarkably, although the investigators administered only what they believed would be an amount of [^{67}Cu]2IT-BAT-Lym-1 sufficient for their imaging and dosimetry studies, they achieved good clinical responses in 7 of the 11 subjects who displayed cutaneous lesions, achieving almost a 50% average reduction in lesion size. Further studies by this group compared the therapeutic potential of ^{64}Cu and ^{67}Cu in a hamster model bearing human colon cancers and found that the 2 radionuclides were equivalent in this cell line and animal model (*21*). Although ^{64}Cu is primarily thought of as a positron (β^+)-emitting radionuclide for PET imaging, the branching ratio for positrons is only 17% whereas ^{64}Cu also emits β^- particles with 39% abundance.

To the best of our knowledge, the data reported in this work represent the first documented use of combined ^{64}Cu and ^{67}Cu as a clinical theranostic pair in humans. The pairing of ^{64}Cu with ^{67}Cu has been used firstly to confirm and localize tumor targeting in the subjects (with ^{64}Cu) and subsequently to deliver the therapeutic product (with ^{67}Cu). Administration of almost identical diagnostic and therapeutic drug products using the different radioisotopes of copper for each role represents the ideal same-element theranostic pairing. The use of different-element theranostic pairs such as ^{68}Ga or ^{111}In for imaging paired with either ^{90}Y or ^{177}Lu for therapy has been shown to potentially alter the biodistribution of the product between imaging and therapy (*22*). The imaging data in this paper provide a high level of confidence that the targeting seen in the PET study will truly reflect the therapeutic radiopharmaceutical delivery and retention, hence demonstrating a particularly attractive characteristic of the copper pairing (Fig. 3).

Compared with conventional radionuclides (e.g., ^{18}F, ^{68}Ga) for diagnostic imaging PET, which have physical half-lives of less than 2 h, the longer half-lives of the copper radionuclides used here have several advantages. One is that both SARTATE products can potentially be radiolabeled in a centralized, good-manufacturing-practice–licensed facility and transported to the clinical center for use. In our case, the [^{64}Cu]Cu-SARTATE product is manufactured in Adelaide, South Australia, and flown overnight to Sydney, New South Wales, a distance of approximately 1,200 km. Centralized manufacture obviates investment in expensive radiopharmaceutical synthesis equipment by the local PET facility, along with the staff required to perform the radiolabeling, production, and quality assurance of the PET radiopharmaceutical. The [^{67}Cu]Cu-SARTATE can be made in the same production facility and transported in an identical manner. However, for this early proof-of-principle trial, we chose to perform the radiolabeling locally on-site because the ^{67}Cu was produced in Idaho and required several flights to be transported the 13,000 km to Sydney, with the half-life of just over 60 h being a consideration.

The effective dose of the most commonly used somatostatin receptor type 2–targeting PET radiopharmaceutical, [^{68}Ga]Ga-DOTA-octreotate, is 4.2 mSv for 200 MBq (*23*). The trial design used here was informed by previous preliminary dosimetry estimates using [^{64}Cu]Cu-SARTATE in subjects with neuroendocrine tumors (*4*); that previous work reported a whole-body effective dose of 4.5×10^{-2} mSv/MBq, or approximately 9 mSv per 200 MBq. Previously, dose estimates in major organs for a different

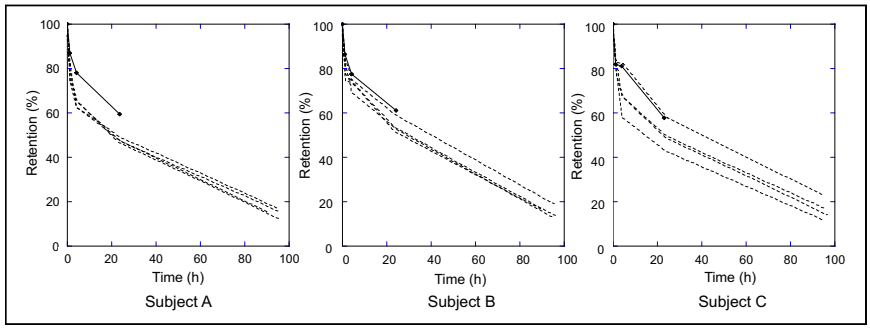

FIGURE 4. Whole-body retention determined from PET and SPECT imaging is shown for each subject. PET retention of [^{64}Cu]Cu-SARTATE is shown as solid line, whereas dashed lines are for each of 4 cycles of [^{67}Cu]Cu-SARTATE measured to approximately 96 h after treatment. Curves are corrected for radionuclide decay and normalized to amount of radiopharmaceutical administered (100%). [^{64}Cu]Cu-SARTATE retention remains on upper side of [^{67}Cu]Cu-SARTATE retention curves in all cases, possibly reflecting influence that coadministered amino acid infusion on treatment day has on retention of [^{67}Cu]Cu-SARTATE.

TABLE 2
Average [^{67}Cu]Cu-SARTATE Biodistribution Data

Parameter	Scan time point 1	2	3	4
Hours from infusion	1	4	24	96
Site				
Adrenals	0.05	0.05	0.04	0.02
Heart contents	0.39	0.26	0.19	0.02
Liver	8.7	8.6	4.4	1.9
Lungs	2.8	2.3	1.5	0.5
Kidneys	4.5	4.1	3.0	1.1
Lower large intestine	0.47	0.38	0.51	0.21
Pancreas	1.23	0.91	0.53	0.04
Red marrow	1.6	1.5	1.2	0.4
Small intestine	2.2	2.3	1.7	0.6
Spleen	2.8	3.1	2.4	0.7
Urinary bladder	5.6	1.3	1.5	0.6
Remainder of body	69.6	63.2	47.9	14.7
Total	100.0	88.0	64.9	20.7

Data are percentage injected dose (%ID) per organ for all 3 subjects over all 4 treatment cycles (values corrected for radioactive decay) at each time point.

TABLE 3
Organ-Absorbed Doses from [^{64}Cu]Cu-SARTATE and [^{67}Cu]Cu-SARTATE

Organ	Mean absorbed dose (mGy/MBq) [^{64}Cu]Cu-SARTATE	[^{67}Cu]Cu-SARTATE	^{67}Cu/^{64}Cu ratio (mGy)
Adrenals	8.30×10^{-2}	1.79×10^{-1}	2.2
Brain	1.29×10^{-2}	4.12×10^{-2}	3.2
Breasts	1.32×10^{-2}	3.85×10^{-2}	2.9
Gallbladder wall	2.42×10^{-2}	5.43×10^{-2}	2.2
LLI wall	3.68×10^{-2}	1.13×10^{-1}	3.1
Small intestine	5.00×10^{-2}	1.58×10^{-1}	3.2
Stomach wall	2.07×10^{-2}	4.88×10^{-2}	2.4
ULI wall	2.00×10^{-2}	5.14×10^{-2}	2.6
Heart wall	2.06×10^{-2}	5.42×10^{-2}	2.6
Kidneys	2.46×10^{-1}	5.45×10^{-2}	2.2
Liver	9.90×10^{-2}	1.73×10^{-1}	1.7
Lungs	3.85×10^{-2}	8.50×10^{-2}	2.2
Muscle	1.56×10^{-2}	2.54×10^{-2}	1.6
Ovaries	1.79×10^{-2}	4.85×10^{-2}	2.7
Pancreas	4.12×10^{-2}	7.98×10^{-2}	1.9
Red marrow	2.11×10^{-2}	6.19×10^{-2}	2.9
Osteogenic cells	3.22×10^{-2}	1.30×10^{-1}	4.0
Skin	1.20×10^{-2}	3.66×10^{-2}	3.0
Spleen	4.78×10^{-1}	6.42×10^{-1}	1.3
Testes	1.19×10^{-2}	4.08×10^{-2}	3.4
Thymus	1.46×10^{-2}	4.08×10^{-2}	2.8
Thyroid	1.35×10^{-2}	5.34×10^{-2}	3.9
Urinary bladder wall	3.81×10^{-2}	6.22×10^{-2}	1.6
Uterus	1.77×10^{-2}	5.23×10^{-2}	3.0
Total body	2.32×10^{-2}	5.19×10^{-2}	2.2

LLI = lower large intestine; ULI = upper large intestine.
Data are mean of 3 subjects. [^{67}Cu]Cu-SARTATE estimates are based on all 4 cycles estimated independently in each subject and then averaged across all 3 subjects. Mean effective dose was 3.95×10^{-2} mSv/MBq for [^{64}Cu]Cu-SARTATE and 7.62×10^{-2} mSv/MBq for[^{67}Cu]Cu-SARTATE.

^{64}Cu-labeled somatostatin receptor type 2–targeting agent, [^{64}Cu]Cu-DOTA-octreotate, have been published (*16*). The effective dose of [^{64}Cu]Cu-DOTA-octreotate was reported to be 6.3 mSv for 200 MBq (*16*). The average effective dose measured in the 3 subjects in this trial with [^{64}Cu]Cu-SARTATE was 3.95×10^{-2} mSv/MBq, which equates to approximately 8 mSv for 200 MBq administered, similar to the value reported by Hicks et al. (*4*). The slight increase in the latter potentially reflects the fact that their subjects had metastatic disease, which may affect the estimates. In a PET/CT examination from vertex of skull to mid thigh, the CT contribution is an additional 8–15 mSv (*24*). Therefore, the estimated difference of about 4 mSv between [^{68}Ga]Ga-DOTA-octreotate (4.2 mSv) and [^{64}Cu]Cu-SARTATE (8 mSv) may be deemed acceptable when considering the total dose for the overall combined PET/CT examination.

This article does not include any estimates of the absorbed dose to the intracranial lesions that were the therapeutic targets in this trial, dose–response relationships, or efficacy. One reason is that the limited spatial resolution of SPECT with a medium-energy collimator and current technology is such that the radioactivity contained in any mass or lesion less than approximately 50 mm in cross-sectional dimension will be underestimated (*25*). New approaches to image reconstruction and postprocessing are attempting to address this limitation (*26*). Most organs measured in this study were larger than the intracranial lesions and hence not subject to the same magnitude of underestimation. With the limited number of enrolled subjects, it was felt that dose–response and efficacy, which were secondary endpoints of the trial, would not be reliable to report and that larger series would be required. Lesion dosimetry in the multifocal, metastatic setting currently remains time-consuming but might be improved with new machine-based learning approaches. We have not included [^{64}Cu]Cu-SARTATE estimated dosimetry for the [^{67}Cu]Cu-SARTATE treatment because of the differences in the physiologic conditions under which the respective radiopharmaceuticals were administered (with and without amino acid infusion). Also, there were differences in the imaging technologies due to the large difference in spatial resolution, leading to potential underestimation of the SPECT-based image radiopharmaceutical concentrations in organs and other tissues (*27*). An example can be seen by comparing the lesion sizes in PET and SPECT in Figure 3. This is the subject of further ongoing investigation.

CONCLUSION

To the best of our knowledge, this is the first reported use of [^{64}Cu]Cu-SARTATE and [^{67}Cu]Cu-SARTATE as a theranostic pair. Both compounds were shown to be safe, well-tolerated, and able to be studied over prolonged imaging time points. No life-threatening or serious adverse events were observed, nor were there any adverse events leading to withdrawal from the study or discontinuation of treatment. The matched pairing was shown by PET and SPECT imaging to have identical targeting to tumors for guiding therapy, demonstrating a nearly ideal theranostic product pair. The extended half-life and suitable PET imaging characteristics of ^{64}Cu should allow for personalized dosimetry before treatment—a capability not presently possible with conventional PET imaging radionuclides such as ^{18}F and ^{68}Ga. Further studies will be required to examine the factors influencing the relationship between ^{64}Cu dosimetry and that observed after therapy with ^{67}Cu.

DISCLOSURE

Harry Marquis was funded by a doctoral scholarship from the Sydney Vital Translational Cancer Research Centre (Cancer Institute NSW) and has received travel grant support from Sydney Vital. Clarity Pharmaceuticals (Sydney, Australia) supplied the [^{64}Cu]Cu-SARTATE and [^{67}Cu]Cu-SARTATE used in this clinical trial. Matthew Harris, Colin Biggin, and Michelle Parker are employees and stockholders of Clarity Pharmaceuticals, the sponsor of this study. Dale Bailey has previously served as a member of the Clarity Pharmaceuticals Scientific Advisory Board. No other potential conflict of interest relevant to this article was reported.

KEY POINTS

QUESTION: How do the radiation dosimetry estimates compare between copper-labeled radiopharmaceuticals and conventional PET radiotracers?

PERTINENT FINDINGS: In the 3 individuals in this study, radiation dosimetry from copper-labeled radiopharmaceuticals was comparable to that from other widely used PET radiotracers such as ^{18}F-FDG and ^{68}Ga-labeled peptides. ^{64}Cu and ^{67}Cu were found to be a suitable theranostic pair of radionuclides.

IMPLICATIONS FOR PATIENT CARE: Copper-labeled radiopharmaceuticals are safe to use in diagnostic imaging and for radionuclide therapy. In addition, the fact that the longer physical half-lives of these radiopharmaceuticals allow them to be manufactured in a central radiopharmacy and transported large distances to the PET scanner facility will provide greater access and convenience for patients.

REFERENCES

1. Blower PJ, Lewis JS, Zweit J. Copper radionuclides and radiopharmaceuticals in nuclear medicine. *Nucl Med Biol.* 1996;23:957–980.
2. Yagi M, Kondo K. Preparation of carrier-free ^{67}Cu by the ^{68}Zn(γ,p) reaction. *Int J Appl Radiat Isot.* 1978;29:757–759.
3. Paterson BM, Roselt P, Denoyer D, et al. PET imaging of tumours with a ^{64}Cu labeled macrobicyclic cage amine ligand tethered to Tyr^3-octreotate. *Dalton Trans.* 2014;43:1386–1396.
4. Hicks RJ, Jackson P, Kong G, et al. ^{64}Cu-SARTATE PET imaging of patients with neuroendocrine tumors demonstrates high tumor uptake and retention, potentially allowing prospective dosimetry for peptide receptor radionuclide therapy. *J Nucl Med.* 2019;60:777–785.
5. Dutour A, Kumar U, Panetta R, et al. Expression of somatostatin receptor subtypes in human brain tumors. *Int J Cancer.* 1998;76:620–627.
6. Malinconico M, Boschi F, Asp J, et al. Automated production of Cu-64, Zr-89, Ga-68, Ti-45, I-123 and I-124 with a medical cyclotron, using a commercial solid target system. *Nucl Med Biol.* 2019;72:S6.
7. Francis RJ, Bailey DL, Hofman MS, Scott AM. The Australasian Radiopharmaceutical Trials Network: clinical trials, evidence, and opportunity. *J Nucl Med.* 2021;62:755–756.
8. Willowson K, Bailey DL, Baldock C. Quantitative SPECT reconstruction using CT-derived corrections. *Phys Med Biol.* 2008;53:3099–3112.
9. Hudson HM, Larkin RS. Accelerated image reconstruction using ordered subsets of projection data. *IEEE Trans Med Imaging.* 1994;13:601–609.
10. Meikle SR, Hutton BF, Bailey DL. A transmission dependent method for scatter correction in SPECT. *J Nucl Med.* 1994;35:360–367.
11. Chang LT. A method for attenuation correction in radionuclide computed tomography. *IEEE Trans Nucl Sci.* 1978;NS-25:638–643.
12. Stabin MG, Sparks RB, Crowe E. OLINDA/EXM: the second-generation personal computer software for internal dose assessment in nuclear medicine. *J Nucl Med.* 2005;46:1023–1027.
13. Watson EE, Stabin MG, Siegel JA. MIRD formulation. *Med Phys.* 1993;20:511–514.
14. Cristy M. Active bone marrow distribution as a function of age in humans. *Phys Med Biol.* 1981;26:389–400.
15. Stabin MG. *Fundamentals of Nuclear Medicine Dosimetry.* Springer; 2008:151.
16. Pfeifer A, Knigge U, Mortensen J, et al. Clinical PET of neuroendocrine tumors using ^{64}Cu-DOTATATE: first-in-humans study. *J Nucl Med.* 2012;53:1207–1215.
17. Apelgot S, Coppey J, Gaudemer A, et al. Similar lethal effect in mammalian cells for two radioisotopes of copper with different decay schemes, ^{64}Cu and ^{67}Cu. *Int J Radiat Biol.* 1989;55:365–384.
18. Schwarz SW, Cutler PD, Eichling JI. Tumor dosimetry for Cu-64 and Cu-67-labeled Mab 1A3 for radioimmunotherapy [abstract]. *J Nucl Med.* 1995;36(suppl 5):42.
19. DeNardo SJ, DeNardo GL, Kukis DL, et al. ^{67}Cu-21T-BAT-Lym-1 pharmacokinetics, radiation dosimetry, toxicity and tumor regression in patients with lymphoma. *J Nucl Med.* 1999;40:302–310.
20. DeNardo GL, Kukis DL, Shen S, DeNardo DA, Meares CF, DeNardo SJ. ^{67}Cu- versus ^{131}I-labeled Lym-1 antibody: comparative pharmacokinetics and dosimetry in patients with non-Hodgkin's lymphoma. *Clin Cancer Res.* 1999;5:533–541.
21. Connett JM, Anderson CJ, Guo LW, et al. Radioimmunotherapy with a ^{64}Cu-labeled monoclonal antibody: a comparison with ^{67}Cu. *Proc Natl Acad Sci USA.* 1996;93:6814–6818.
22. Miller C, Rousseau J, Ramogida CF, Celler A, Rahmim A, Uribe CF. Implications of physics, chemistry and biology for dosimetry calculations using theranostic pairs. *Theranostics.* 2022;12:232–259.
23. Walker RC, Smith GT, Liu E, Moore B, Clanton J, Stabin M. Measured human dosimetry of ^{68}Ga-DOTATATE. *J Nucl Med.* 2013;54:855–860.
24. Willowson KP, Bailey EA, Bailey DL. A retrospective evaluation of radiation dose associated with low dose FDG protocols in whole-body PET/CT. *Australas Phys Eng Sci Med.* 2012;35:49–53.
25. Ryu H, Meikle SR, Willowson KP, Eslick EM, Bailey DL. Performance evaluation of quantitative SPECT/CT using NEMA NU 2 PET methodology. *Phys Med Biol.* 2019;64:145017.
26. Marquis H, Deidda D, Gillman A, et al. Theranostic SPECT reconstruction for improved resolution: application to radionuclide therapy dosimetry. *EJNMMI Physics.* 2021;8:16.
27. Marquis H, Willowson KP, Bailey DL. Partial volume effect in SPECT & PET imaging and impact on radionuclide dosimetry estimates. *Asia Ocean J Nucl Med Biol.* 2023;11:44–54.